DFT insights into stress-induced impact on the fundamental properties of $SnPbO_3$ cubic Perovskite oxides for advanced optoelectronic devices

M. I. Khan [a *], M. Riaz [b], B. Ali [c], A. A. Algethami [d], H. T. Ali [d], M. S. U. Sahar [e]
[a] *Institute of Mechanical and Manufacturing Engineering, Khwaja Fareed UEIT, Rahim Yar Khan, 64200, Pakistan*
[b] *Institute of Physics, The Islamia University, Bahawalpur, Pakistan*
[c] *Institute of Chemistry, Khwaja Fareed UEIT, Rahim Yar Khan, 64200, Pakistan*
[d] *Department of Mechanical Engineering, College of Engineering, Taif University, Kingdom of Saudi Arabia*
[e] *Department of Mechanical, Industrial, and Energy Systems, University of Sargodha, Sargodha - 40100, Pakistan*

Inorganic lead-based perovskite oxides have been widely studied in diverse fields because of their extreme structural flexibility and optimization. In this study, geometrical, electronic, optical, mechanical, thermodynamic, phonon density of states (DOS), and EELS analysis for $SnPbO_3$ cubic perovskite oxides were explored under varying stress levels (0–100 GPa) using DFT within the CASTEP code framework. Lattice parameters and unit cell volume exhibit a consistent decline with increasing stress levels. Electronically, the band gap increases sharply from 0.203 to 2.943 eV up to 80 GPa and then decreases from 2.943 eV to 2.894 eV. In the theoretical XRD pattern, a slight shift of peaks up to 60 GPa was observed. The Total Density of States (TDOS), along with the partial DOS, confirmed the contributions of Sn (5s), Pb (5d), and O (2p) orbitals. From optical properties, absorption and reflectivity increase steadily with increasing stress, indicating stronger light interaction, while conductivity only increases up to 60 GPa and then decreases, which may be due to the presence of structural defects. The phonon DOS showed a stress-induced impact on the lattice dynamics, indicating an increase in structural stiffness. Elastic constants (C_{11}, C_{12}, C_{44}) meet the Born stability criteria, confirming the mechanical stability, as supported by the Debye temperature (θD) and more negative free energy. Additionally, the comprehensive analysis of elastic moduli, including Young's modulus, bulk modulus, Pugh ratio, and Frantsevich ratio, along with key mechanical descriptors, further supports that $SnPbO_3$ exhibits more ductile and isotropic behavior at higher stress levels (0–100 GPa). Furthermore, EELS analysis of the constituent elements (Sn, Pb, and O) regarding their absorption and emission behavior confirmed their relative stability under higher stress and showed a prominent electronic structure. These findings highlight the potential of $SnPbO_3$ perovskite oxide materials under varying stress (0–100 GPa) for advanced optoelectronic devices.

(Received April 21, 2025; Accepted July 15, 2025)

Keywords: Perovskite oxides, DFT, Elastic properties, Optoelectronic devices

1. Introduction

Perovskite oxide materials (ABO_3) have become the focal point of material researchers and have gained substantial consideration in diverse areas due to their remarkable multifunctional properties, such as good electronic conductivity, magnetism, optical absorption, and catalytic activity [1]. These materials are key players in numerous advanced applications, including photovoltaics, energy storage, solid oxide fuel cells, ferroelectric, piezoelectric technologies for sensors, and high-temperature superconductors [2]. Among these materials, tin (Sn)-based perovskite oxides have emerged as particularly promising candidates due to their unique properties that cater to both energy and electronic applications [3]. Their eco-friendly nature addresses

* Corresponding author: ijazkhan4123@gmail.com
https://doi.org/10.15251/JOR.2025.214.431

environmental concerns, especially in the context of sustainable energy solutions like photovoltaics and optoelectronics [4]. The tunable oxidation states of Sn contribute to its excellent electronic conductivity and improve charge carrier mobility, which is crucial for developing high-performance solar cells [5]. Their intrinsically narrow band gap enables superior light absorption, particularly across the visible and infrared regions of the spectrum. Additionally, the structural and chemical flexibility permits tuning the properties through doping or compositional modifications, enhancing their performance and stability in various conditions [6]. While efficiency is still behind the top-performing perovskites, it remains an attractive option, and researchers continue to explore ways to improve their stability and performance. On the other hand, lead-based perovskite oxides have been extensively studied for their diverse range of properties, including high dielectric constant, strong piezoelectric characteristics, good thermal stability, and significant responsiveness to mechanical stress [7]. These characteristics make them useful in various applications. However, despite these desirable properties, the use of lead (Pb) has raised environmental concerns due to its inherent toxicity, prompting a shift towards developing lead (Pb)-free alternatives, such as tin-based perovskites, which aim to provide similar functionalities while being more environment-friendly [8]. The pursuit of eco-friendly materials becomes the dynamic focus in the advancement of perovskite technology. Lead (Pb), being a heavy and malleable metal, has been used in lead-acid batteries, photovoltaic cells, photocatalytic applications, alloys, ceramics, and radiation shielding [9]. In particular, carbon-based technologies have been shown to enhance the performance of lead-acid batteries. In the energy storage sector, over 80% of the total annual lead (Pb) produced worldwide is used in lead-acid batteries. Incorporating Density Functional Theory (DFT) into research offers significant advantages over experimental work, particularly in terms of predictive capabilities, cost-effectiveness, and atomic-level insights [10]. DFT enables researchers to simulate material properties with high precision before synthesis, saving time and resources by identifying promising candidates. Additionally, DFT offers flexibility in exploring hypothetical materials and can be used to investigate extreme conditions that may be challenging to replicate experimentally, accelerating material discovery through rapid screening of potential candidates.

Many researchers have explored different materials under stress conditions. Some of these are: Zaidi et al. explored stress effects (0–100 GPa) on $SrHfO_3$, revealing significant property changes and mechanical stability, highlighting its semiconductor potential [11]. Md Rajib et al. investigated the fundamental properties of perovskite oxides $BeZrO_3$, using PBE, RPBE, LDA, and B3LYP functional for absorbing visible light efficacy [12]. N. A. Noor et al. explored the potential of perovskite oxides $ZnZrO_3$ under applied pressure ranging from 0 to 20 GPa using PBEsol-GGA approximation for thermoelectric devices [13]. Parvaiz and his colleagues studied CsXO3 (X = Ti, Mn, and Cu) inorganic perovskite oxides for photosensitive applications [14]. Shakeel et al. performed an in-depth theoretical analysis of $PbTaO_3$ perovskite oxides under applied stress ranging from 0 to 30 GPa, which exhibited metallic behavior [15]. Abu Bakar et al. theoretically confirmed the mechanical stability of cubic perovskites $XCoO_3$ (X = Nd, Pr) under varying stress, suggesting their suitability for high-temperature devices [16].

$SnPbO_3$ has captivated attention as an intriguing material. To our knowledge, very little research has been conducted on this material. Specifically, no study, either theoretical or experimental, has explored the potential of the considered perovskite oxide at varying stress from 0 to 100 GPa, motivating us to address this gap. Understanding the electronic-level synergistic effects of $SnPbO_3$ is crucial for unlocking its potential across a wide range of applications. The combination of distinct oxidation states in Sn and Pb gives $SnPbO_3$ distinctive structural and electronic characteristics, positioning it as an outstanding candidate for next-generation technological innovations. In this study, we use density functional theory (DFT) to examine the structural, electronic, optical, elastic, and mechanical characteristics of $SnPbO_3$, along with theoretical XRD analysis under applied stress ranging from 0 to 100 GPa. Our findings aim to shed light on the exciting possibilities that $SnPbO_3$ presents for the future of perovskite materials in advanced photovoltaic technologies.

2. Computational details

The entire density functional theory (DFT) computation for $SnPbO_3$ was performed within the CASTEP simulation package [17]. The unit cell was considered to be a 1×1×1 cubic structure with space group pm3m (221), and a 2×2×2 supercell was used for a theoretical X-ray diffraction (XRD) study. The electron-ion interactions were simulated using a plane-wave basis with a 340 eV cutoff energy and ultrasoft pseudopotentials, and exchange-correlation effects were described by the PBE-GGA functional [18]. A 4×4×4 Monkhorst-Pack k-point grid was used to sample the Brillouin zone, with self-consistent field (SCF) convergence achieved at a threshold of 1×10^{-6} eV per atom [19]. The band energy convergence criterion was established at 1×10^{-5} eV, and structural optimization was performed using the Broyden–Fletcher–Goldfarb–Shanno (BFGS) algorithm [20], with Pulay mixing applied to ensure efficient electronic structure convergence [21]. Fig. 1 illustrates the visualization of the $SnPbO_3$ unit cell.

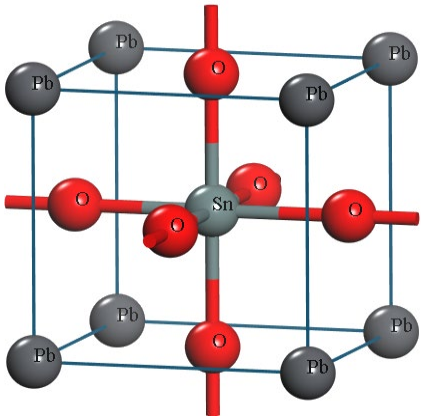

Fig. 1. A unit cell structure of $SnPbO_3$.

3. Results and discussion

3.1. Geometrical properties

This study investigates the stress-induced variations (0 to 100 GPa) on the lattice parameters and volume of the $SnPbO_3$ perovskite oxide, which are critical for understanding its physical properties [22]. The lattice parameter exhibited a pronounced decrement from an initial value of 4.2 Å at 0 GPa to 3.8 Å at 100 GPa, as shown in Fig. 2. This marked reduction highlights the compressive effect of external stress on the crystal structure, commonly referred to as lattice compression [23]. Similarly, the reduction in unit cell volume from 4.3 $Å^3$ to 3.81 $Å^3$ was observed as the stress increased from 0 to 100 GPa, further emphasizing the material's compressive response [24]. This phenomenon is consistent with the general tendency of materials under stress, where interatomic distances are reduced due to the tight packing of atoms within the crystal lattice [25].

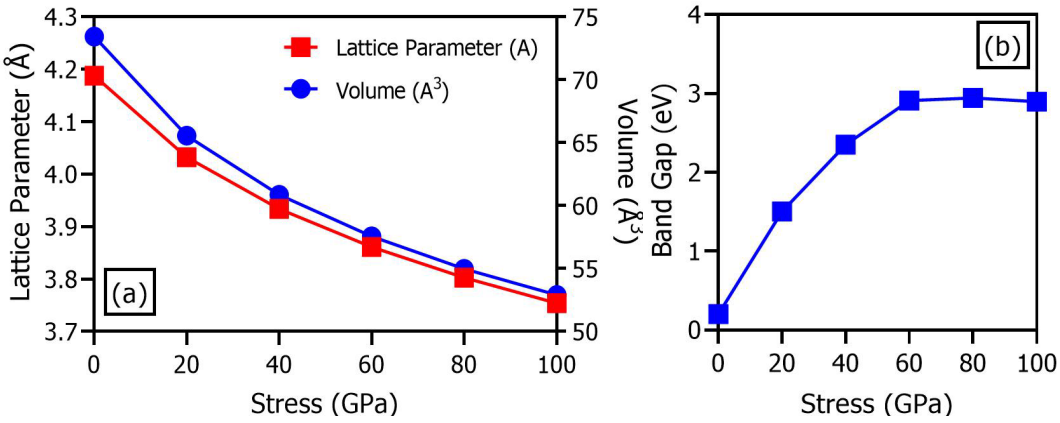

Fig. 2. (a) Lattice parameters and unit cell volume, (b) Band gap of $SnPbO_3$ with varying stress (0–100 GPa).

Fig. 3 displays the theoretical XRD patterns of the $SnPbO_3$ perovskite oxide under varying stress conditions. The diffraction peaks align closely with the JCPDS card no. 11-23-814, confirming the cubic $SnPbO_3$ phase [26]. However, as the stress increases, the diffraction peaks consistently shift slightly toward higher 2θ angles, indicating a decrease in lattice parameters and unit cell volume caused by the compression of the crystal structure, which further validates the reliability of the results [27]. Despite the shifting, the peak intensity remains stable, signifying that the crystal structure integrity of $SnPbO_3$ is preserved across the stress range (0–100GPa).

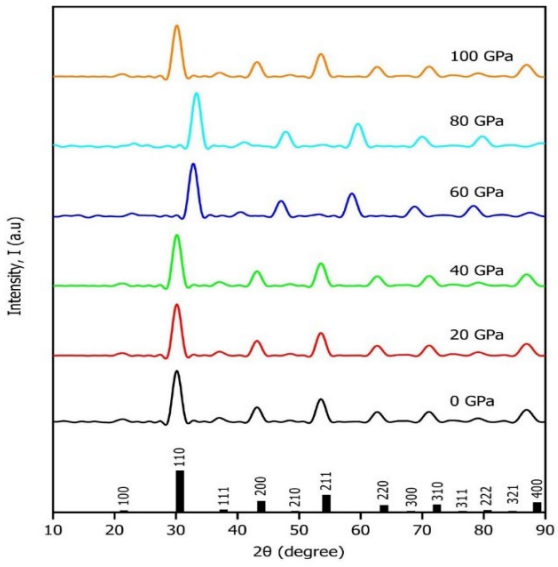

Fig. 3. Theoretical XRD pattern of $SnPbO_3$ with varying stress (0–100 GPa)

3.2. Electronic properties

Fig. 4(a–f) illustrates the detailed analysis of the electronic properties of the $SnPbO_3$ perovskite oxide as a function of applied stress from 0 to 100 GPa. Under applied stress, the band gap widened significantly, increasing from 0.02 eV at 0 GPa to 1.5 eV at 20 GPa, and further to 2.35 eV at 40 GPa. Notably, the band gap reached its maximum value of 2.94 eV at 80 GPa, before slightly decreasing to 2.89 eV at the higher stress level of 100 GPa, as shown in Figure 4. Under stress, the atomic arrangement within the material undergoes modifications, resulting in a shift in the electronic band structure [28]. The increased band gap reflects the widening separation and

signifies an increased energetic barrier for electron excitation, indicating a greater separation between the valence and conduction bands under applied stress [29]. This reduction in electron mobility is characteristic of insulating materials and suggests that under higher stress conditions, the material becomes less conductive. The widening of the band gap is indicative of a transition from semiconductor-like behavior to insulating behavior as stress increases [30].

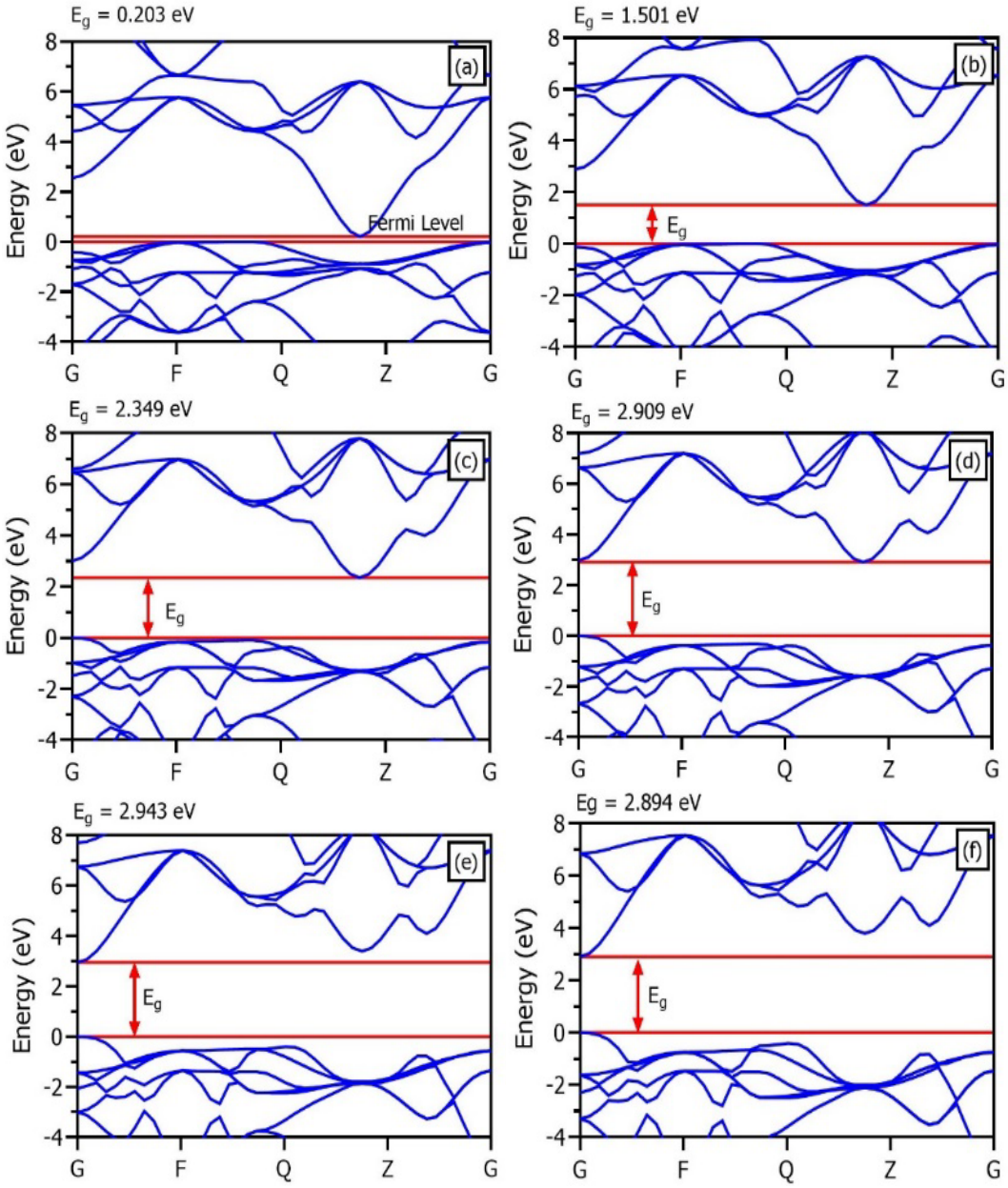

Fig. 4. (a–f) bang gap of $SnPbO_3$ with varying stress (0–100 GPa).

The density of states (DOS) provides a numerical description of the distribution of electronic states and permits a deeper understanding of a material's electronic structure and its associated physical properties [31]. Figure 5(a–d) illustrates the total and partial density of states (DOS) of the $SnPbO_3$ perovskite oxide under applied stresses from 0 to 100 GPa, highlighting the dominant electronic contributions from the Sn 5s, Pb 5d, and O 2p orbitals. These partial contributions may affect the band gap, thereby influencing the optical and electrical behaviors of $SnPbO_3$ under stress conditions [32].

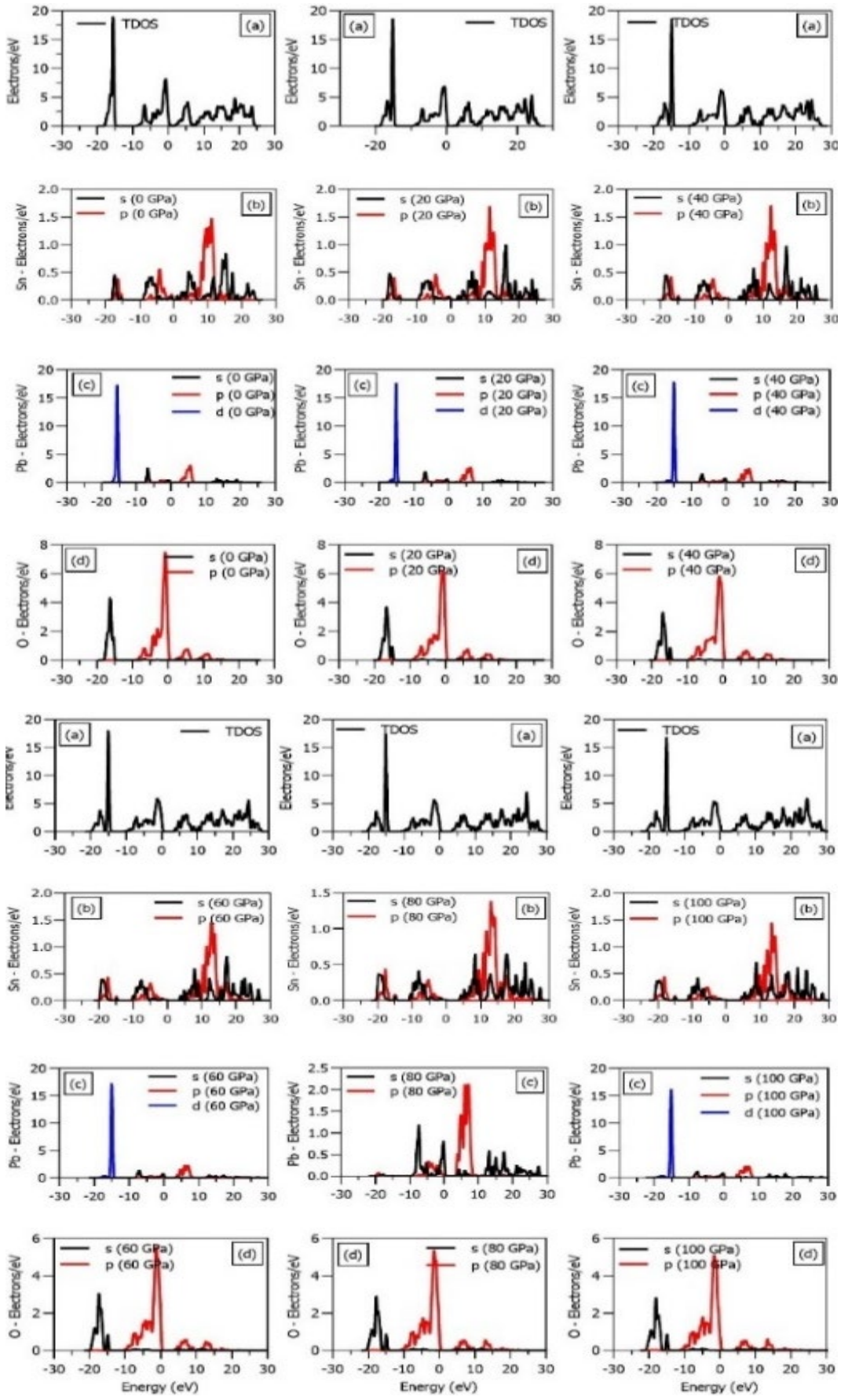

Fig. 5. TDOS of $SnPbO_3$ with varying stress (0–100 GPa).

3.3. Optical characteristics

The optical properties are fundamental for probing the stress-dependent behavior, which provides essential insights for the rational design of materials with optimized optical performance [33]. The characteristic profiles at varying stress levels are shown in Figure 6(a–f). From Figure 6(a), at 0 GPa, the absorption was measured at 6×10^{-5} cm^{-1}. As the applied stress increased to 20 GPa, the absorption increased to 6.5×10^{-5} cm^{-1}, and at 40 GPa, it further increased to 7×10^{-5} cm^{-1}. This trend continued, with absorption reaching 8×10^{-5} cm^{-1} at 60 GPa, 8.5×10^{-5} cm^{-1} at 80 GPa, and finally 9×10^{-5} cm^{-1} at 100 GPa. The significant increase in the absorption band with rising stress levels demonstrates the material's enhanced capacity to absorb photons over a broader energy range [34]. This phenomenon is attributed to stress-induced modifications in the material's electronic structure and band alignment, which improve photon absorption efficiency [35]. In Figure 6(b), at 0 GPa, the conductivity was found to be 8 eV. As stress increased to 20 GPa, the conductivity reached 10 (1/fs) and further increased to 13 (1/fs) at 40 GPa. By 60 GPa, the conductivity reached its peak at 14 eV. However, as stress continued to rise, conductivity began to decline, dropping to 13.5 eV at 80 GPa and further to 13 eV at 100 GPa. The initial increase from 0 to 60 GPa can be attributed to stress-induced modifications in the material's electronic band structure. As stress is applied, the atomic arrangement shifts, leading to changes in electronic states that enhance charge transport and photon response, resulting in higher conductivity [36]. However, the subsequent decline beyond 80 GPa suggests that excessive stress may lead to the formation of defects or structural changes that degrade its electronic properties.

The dielectric functions (both real and imaginary parts) are key parameters for understanding the optical response, as depicted in Figure 6(c). Across the entire stress range (0–100 GPa), the real dielectric function consistently exhibited maximum values at 0 eV, indicating strong polarization at zero energy levels. It also showed minimum values for all imaginary values, signifying that the material does not absorb energy in this range. As energy increased from 4 to 5 eV, the slope of the real dielectric function decreased and then increased for stress values from 0 GPa to 100 GPa, peaking at a stress value of 40 GPa. This suggests that the material's polarizability and its ability to respond to external electromagnetic fields are most pronounced in this energy range. In contrast, the imaginary component displayed a peak between 5 to 6 eV for all stress levels, indicating a maximum in absorption. Beyond this energy range, the imaginary function remained slightly higher than the real function. This behavior implies that the material becomes more absorptive at higher energies, with a tendency to absorb more energy than it reflects or transmits. The loss function shown in Figure 6(d) exhibits a decrement as stress rises.

Reflectivity peaks showed notable variations in both position and width as stress increased, illustrated in Figure 6(e). At higher stress levels, particularly at 100 GPa, the peaks become broader compared to those observed in lower stress conditions (0 GPa). Despite these variations, the maximum peak heights consistently occur within a narrow energy range of 38 to 48 eV, signifying a strong and stable optical response. From Figure 6(f), the refractive index consistently reached its maximum at 0 eV for all stress levels, indicating that at low energies, the material has a strong impact on the behavior of incident light. As stress levels increased, the refractive index gradually decreased from its maximum value at 0 eV, signifying stress-induced structural changes in the material. The higher stress levels correspond to higher refractive indices overall, reflecting the material's enhanced ability to refract light as stress increases [37].

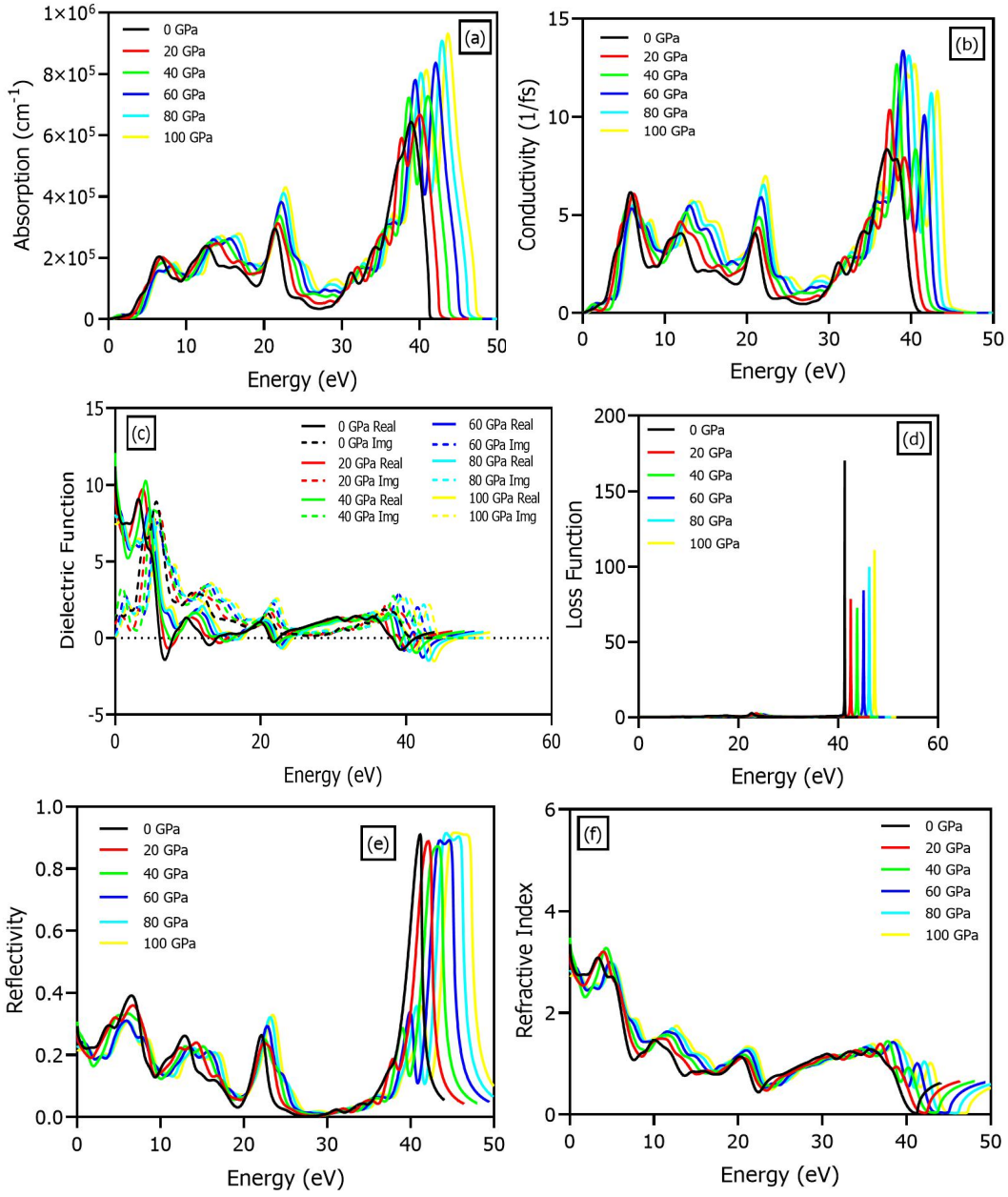

Fig. 6. Stress-dependent(0–100 GPa) optical properties of $SnPbO_3$: (a) absorption, (b) conductivity, (c) dielectric function, (d) loss function, (e) reflectivity, and (f) refractive index.

3.4. Electron energy loss spectroscopy (EELS) analysis

The EELS spectra for all constituent elements, such as Sn, Pb, and O, were simulated, as depicted in Figure 7. The spectra in Figures 7(a–c) provide insights into the energy absorption and emission characteristics of each element under different stress conditions, along with contributions from specific electronic substates [38]. For tin (Sn), the absorption band spans the 0 to 40 eV range, likely linked to the excitation of electrons from the 5s and 5p states of Sn. As stress increased, the absorption band shifted to higher energy, indicating that under higher stress, more energy is required to excite electrons [39]. The emission bands shown in Figure 7(d–f) imply that the capacity of tin (Sn) to emit photons remained unaffected by stress, as the energy was released from higher to lower states.

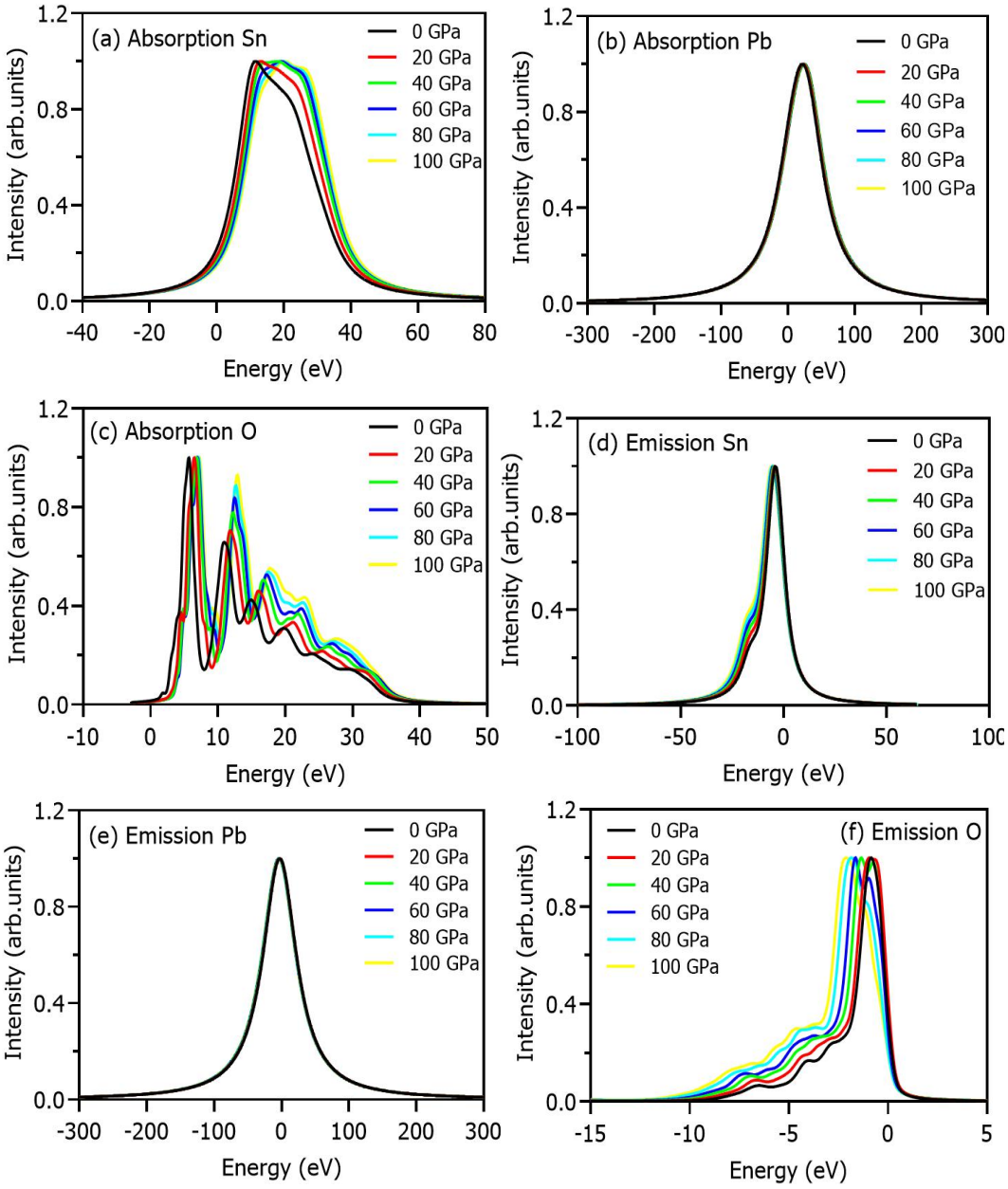

Fig. 7. EELS analysis, (a–c) absorption, and (d–f) emission of the constituent elements at varying stress (0–100 GPa).

For lead (Pb), the absorption band spans from –50 eV to 100 eV, indicating that Pb can absorb energy across a wide energy range and facilitate electron excitation to higher energy levels under various stress conditions due to the 6s, 6p, and 5d states of Pb. Additionally, Pb confirmed notable stability in emission intensity across all stress conditions, with emission maxima consistently occurring at 0 eV. This stability can be attributed to the robust crystal lattice of Pb, which remains structurally intact, and the 6p to 6s transitions likely contribute to the observed stability in emission, as these states remain relatively unaffected by stress. For the oxygen (O) atom, absorption occurs within two specific energy ranges: around 8 eV and from 12 to 20 eV, which are related to transitions from the 2s and 2p states of oxygen. Stress-driven variations in the energy loss spectrum reveal modifications to the 2p orbital energies, which can be attributed to transitions from the 2p orbital to lower energy levels.

4. Mechanical properties

The variation of elastic constants (C_{11}, C_{12}, C_{44}) as a function of applied stress (0–100 GPa) is depicted in Figure 8. All the elastic constants exhibit a pronounced positive correlation over the entire stress range and satisfy the Born stability criteria: $C_{11} - C_{12} > 0$, $C_{11} + 2C_{12} > 0$, and $C_{44} > 0$, confirming the elastic stability of $SnPbO_3$ perovskite oxide [40]. The constant C_{11} linearly increased with applied stress, indicating enhanced resistance to deformation in the axial direction [41]. Both C_{12} and C_{44} demonstrate relatively minor increments, indicating consistent lateral and shear properties under high-stress conditions.

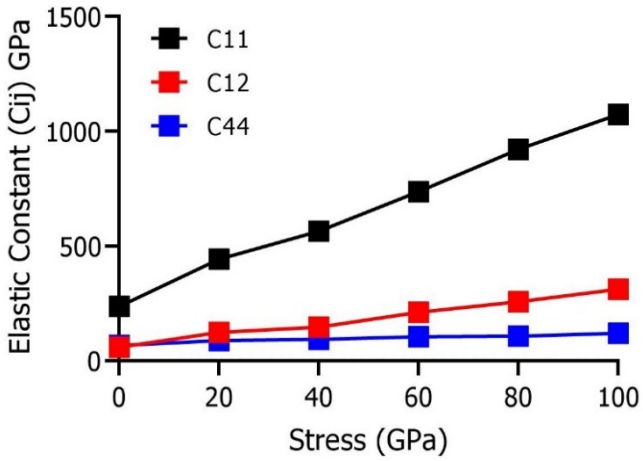

Fig. 8. Elastic constants of $SnPbO_3$ with varying stress (0–100 GPa).

The set of graphs shown in Fig. 9(a–d) provides insights into bulk, shear, and Young's moduli under increasing stress from 0 GPa to 100 GPa, which were computed by employing the literature relation [42]. The bulk modulus is a fundamental mechanical property that measures resistance to uniform compression under applied stress [43]. As shown in Fig. 9(a), the trend exhibits a consistent linear increase as stress levels increase from 0 GPa to 100 GPa. This behavior results from the progressive stiffness of the atomic structure, which led to the observed increase in bulk modulus. Young's modulus shows a proportional response, signifying an increase in stiffness with increasing stress [44]. The initial Young's modulus value at 0 GPa represents the material's intrinsic stiffness under normal conditions. As stress is gradually applied, the material's atomic structure likely becomes stiffer, resulting in enhanced resistance to volume reduction [45]. The shear modulus also increases with increasing stress, though at a slower rate compared to the bulk modulus. This indicates that while the material becomes stiffer under shear stress, its resistance to shear deformation is less pronounced than its resistance to uniform compression. Additionally, a similar trend was observed in Young's modulus and bulk modulus, further supporting the results [46].

The trend of the Pugh ratio and Frantsevich ratio is shown in Fig. 9(b). The Pugh ratio increases steadily from around 1.5 to 3.0, indicating that the material becomes more ductile with increasing stress. On the other hand, the Frantsevich ratio decreases as stress increases, suggesting that the material becomes ductile under higher stress [47]. The Cauchy pressure plotted as a function of stress (0 to 100 GPa) shows a clear upward trend as depicted in Fig. 9(c). The positive trend indicates that the material transitions toward more ductile behavior under higher stress. Finally, the graph of Poisson's ratio and anisotropy factor is shown in Fig. 9(d). Poisson's ratio starts at approximately 0.25 and gradually increases to around 0.37 as stress increases, indicating that the material becomes more isotropic and resistant to volume change under higher stress. Concurrently, the anisotropy factor decreases with increasing stress, smoothing off around 0.4, suggesting that, as stress is applied, the material becomes more isotropic and less directionally dependent in its mechanical behavior.

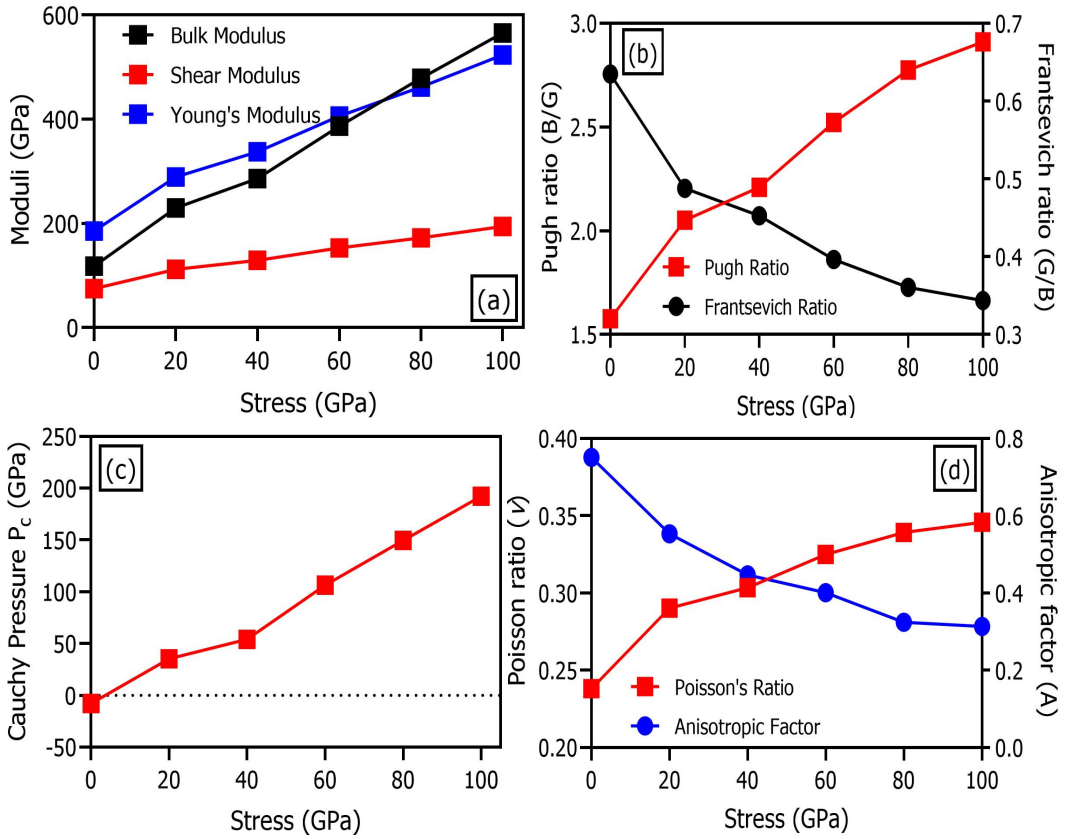

Fig. 9. Variation of moduli and ratios under applied stress (0–100 GPa).

5. Phonon DOS

The phonon DOS of $SnPbO_3$, shown in Fig. 10 over the 0–40 THz frequency range and 0–100 GPa stress levels, provides insights into its thermal and mechanical characteristics, which hypothetically point to phase transitions [48]. At 0 GPa, some peaks are predominantly in the lower frequency region, demonstrating the existence of low-energy quanta vibrational modes associated with relatively weak interatomic bonding and larger atomic displacements. As the stress increases up to 20 GPa and beyond, a significant shift to the higher frequency region is noted. Particularly at 80 GPa and 100 GPa, the phonon DOS broadens substantially, signifying stiffness of phonon modes due to increased interatomic interactions under compression. The increasing stress compresses the atomic lattice, enhancing bond stiffness, which primes to higher vibrational frequencies [49]. Additionally, the distribution of DOS becomes broader, reflecting changes in the phonon spectrum as the material structure adapts to higher stress. At 100 GPa, peaks at higher frequencies are seen to be more dominant, signifying the material's pointedly transformed vibrational properties. Furthermore, the narrow region of certain low-frequency peaks under higher stress replicates the suppression of soft modes, which may indicate a greater degree of structural stiffness. This interplay between peak shifts and broadening as stress increases provides a persuasive sign for the stress-induced evolution of lattice dynamics within the material. Such a shift in phonon behavior has profound implications for thermal conductivity, dynamical stability, and potential electronic-phononic coupling schemes.

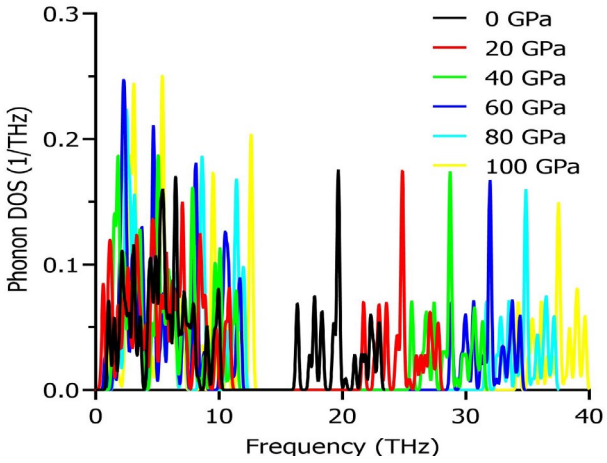

Fig. 10. Phonon DOS for $SnPbO_3$ under applied stress (0–100 GPa).

6. Thermodynamic properties

The thermodynamic behavior across the stress range (0–100 GPa) as a function of temperature is examined, and the trends are depicted in Fig. 11(a–e). The enthalpy and entropy, as depicted in Fig. 11(a) and Fig. 11(c), show a linear trend with temperature. The maximum value of enthalpy was observed at 0.9 cal/cell·K at 1000 K, while the entropy reached about 2.3 eV at the same temperature. Increasing stress slightly reduces entropy values, emulating restricted vibrational freedom under compression [50], as thermal oscillations introduce more disorder [51]. Fig. 11(b) exhibits that free energy decreases with temperature for all stress conditions, and a higher value is observed at –1.8 eV, representing enhanced thermodynamic stability at higher stress levels due to enhanced bonding contacts and constrained atomic vibrations under compression [52]. In Fig. 11(d), heat capacity also increases with higher stress and approaches saturation at higher temperatures, consistent with the Dulong-Petit limit, and shows minimal decline of about 20–35 cal/cell·K under higher stress because of reduced anharmonicity of atomic vibrations under compression. Lastly, the Debye temperature (θD), as shown in Fig. 11(e), decreases with increasing temperature but increases linearly under higher stress conditions, signifying stiffer phonon modes and enhanced vibrational frequencies due to compressional effects [53]. These competing results highlight the significant influence of increasing stress on the thermal and mechanical stability of the material.

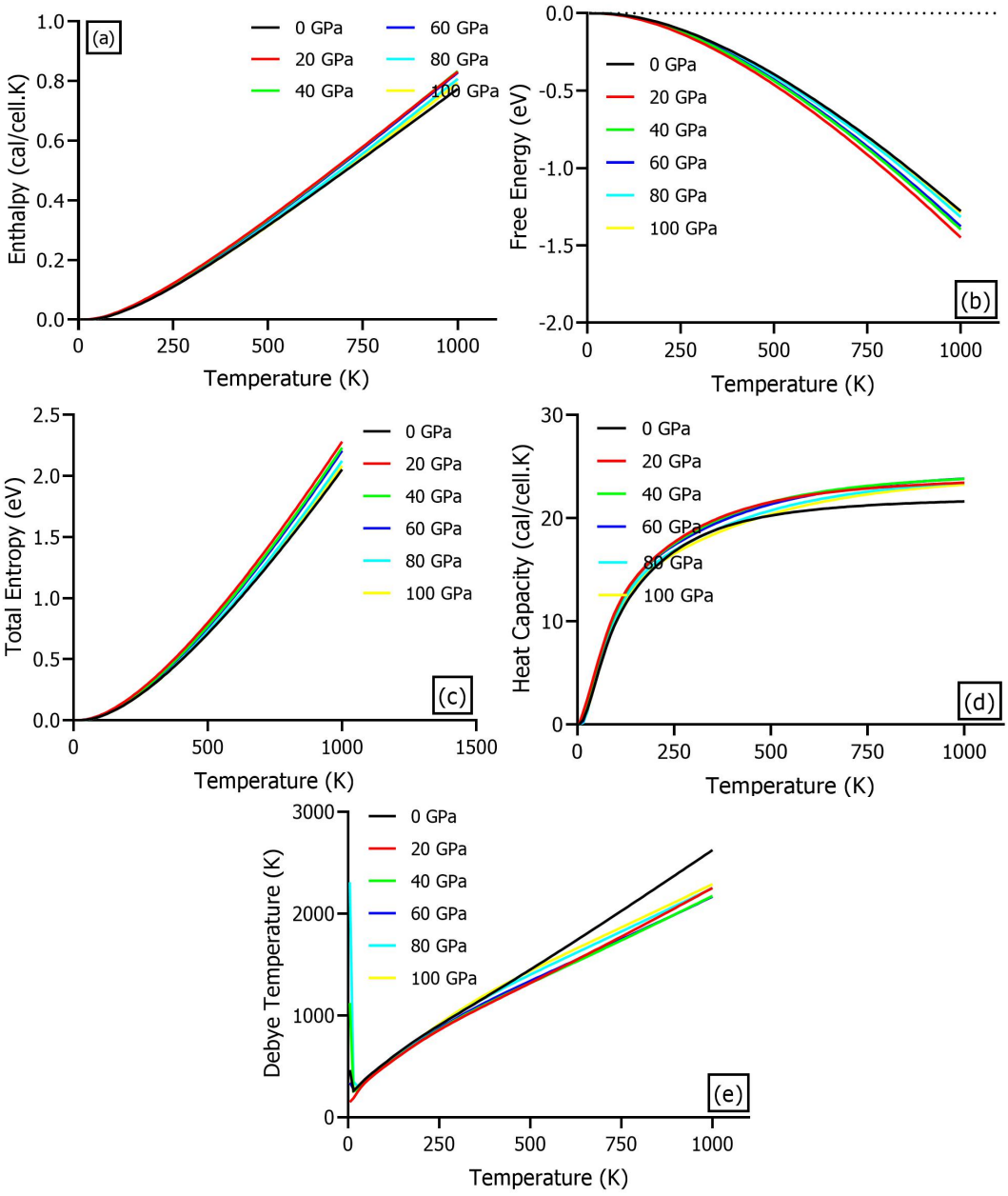

Fig. 11. Thermodynamic parameters of $SnPbO_3$ under stress: (a) enthalpy, (b) Gibbs free energy, (c) entropy, (d) heat capacity, and (e) Debye temperature.

7. Conclusions

Recent studies using DFT within the CASTEP framework have provided valuable insights into how $SnPbO_3$ cubic perovskite oxides behave under different stress levels ranging from 0 to 100 GPa. The theoretical X-ray diffraction patterns confirm that the material maintains its cubic structure, with slight shifts in the peaks observed up to 60 GPa, indicating how it responds to mechanical pressure. The analysis of the Total Density of States (TDOS) and partial Density of States (DOS) shows that the electronic properties are significantly influenced by the Sn (5s), Pb (5d), and O (2p) orbitals. This complexity in electronic structure is linked to the optical properties, which reveal that absorption and conductivity increase as stress is applied. This opens up exciting possibilities for using $SnPbO_3$ in advanced optoelectronic devices. Additionally, the phonon density of states indicates that the material becomes stiffer under stress.

Interestingly, while the elastic constants confirm that the material remains stable, they also suggest that it becomes more ductile and isotropic at higher stress levels. This combination of stability and flexibility presents new research opportunities. EELS analysis shows that the electronic structures of Sn, Pb, and O remain stable even under high stress. The findings about the Debye temperature and the increasingly negative free energy at higher stress levels further support the idea that $SnPbO_3$ is thermodynamically stable. Overall, this research highlights the promising potential of $SnPbO_3$ for advanced optoelectronic applications, particularly due to its robust performance under diverse stress conditions. The insights gained from this study pave the way for further exploration of $SnPbO_3$ in flexible electronics and high-performance materials. Future research could delve deeper into the relationship between mechanical stress and electronic properties, potentially leading to innovative applications that leverage the unique characteristics of $SnPbO_3$. This could include exploring its use in flexible devices that require both mechanical resilience and efficient electronic performance, pushing the boundaries of what is possible in material science and engineering.

Acknowledgement

The authors extend their appreciation to Taif University, Saudi Arabia, for supporting this work through project number (TU-DSPP-2024-285).

Funding

This research was funded by Taif University, Taif, Saudi Arabia, Project No. (TU-DSPP-2024-285).

Declaration of interests

The authors have no conflicts of interest to declare.

Data availability

Research data will be made available upon a reasonable request.

References

[1] W. Xiang, W. Tress, Adv. Mater. 31 (2019) 1902851; https://doi.org/10.1002/adma.201902851

[2] W. Zhang, G.E. Eperon, H.J. Snaith, Nat. Energy 1 (2016); https://doi.org/10.1038/nenergy.2016.48

[3] M. Riaz, S.D. Ali, M. Sadiq, M. Ali, S.M. Ali, Chem. Phys. 577 (2024) 5-8; https://doi.org/10.1016/j.chemphys.2023.112141

[4] L. Zhang, J. Miao, J. Li, Q. Li, Adv. Funct. Mater. 30 (2020); https://doi.org/10.1002/adfm.202003653

[5] A. Grimaud, K.J. May, C.E. Carlton, Y. Lee, M. Risch, W.T. Hong, J. Zhou, Y. Shao-Horn, Nat. Commun. (2013) 1-7; https://doi.org/10.1038/ncomms3439

[6] N.A. Noor, Q. Mahmood, M. Rashid, B. Ul Haq, A. Laref, Ceram. Int. 44 (2018) 13750-13756; https://doi.org/10.1016/j.ceramint.2018.04.217

[7] M. Riaz, T. Munawar, M.S. Nadeem, F. Mukhtar, S.D. Ali, S. Manzoor, M.N. Ashiq, F. Iqbal, J. Appl. Electrochem. (2022); https://doi.org/10.1007/s10800-022-01809-4

[8] H. Chermette, Coord. Chem. Rev. 178-180 (1998) 699-721; https://doi.org/10.1016/S0010-8545(98)00179-9

[9] P. Kumari, R. Sharma, U. Lilhore, R. Khenata, V. Srivastava, Int. J. Energy Res. 46 (2022) 23893-23907; https://doi.org/10.1002/er.8687

[10] S. Cite, Physica B, 649 (2023) 1-5; https://doi.org/10.1016/j.physb.2022.414355

[11] S.M.J. Zaidi, M.S. Ullah, S. Mansoor, M.I. Khan, M. Faizan, M. Hashim, Results Opt. 13 (2023) 100519; https://doi.org/10.1016/j.rio.2023.100519

[12] M.R. Munshi, M. Al Masud, A. Khatun, Phys. Scr. 99 (2024) 1-5; https://doi.org/10.1088/1402-4896/ad5884

[13] N.A. Noor, M. Rashid, G.M. Mustafa, M.I. Khan, A. Mahmood, S.M. Ramay, Chem. Phys. Lett. 753 (2020) 1-18; https://doi.org/10.1016/j.cplett.2020.137601

[14] M.M. Parvaiz, A. Khalil, H.I. Elsaeedy, S. Ayub, M.B. Tahir, Optik (Stuttg). 306 (2024) 1-17; https://doi.org/10.1016/j.ijleo.2024.171795

[15] S.A. Khandy, I. Islam, Z.S. Ganai, D.C. Gupta, K.A. Parrey, J. Electron. Mater. 47 (2018) 436-442; https://doi.org/10.1007/s11664-017-5785-1

[16] A. Bakar, A.O. Alrashdi, M.M. Fadhali, A. Afaq, H.A. Yakout, M. Asif, J. Mater. Res. Technol. 19 (2022) 4233-4241; https://doi.org/10.1016/j.jmrt.2022.06.126

[17] H. Arif, M.B. Tahir, B.S. Almutairi, I. Khalid, M. Sagir, H. Elhosiny Ali, H. Alrobei, M. Alzaid, Inorg. Chem. Commun. 150 (2023) 110474; https://doi.org/10.1016/j.inoche.2023.110474

[18] M. Rizwan, I. Iqra, S.S.A. Gillani, I. Zeba, M. Shakil, Z. Usman, M. Rizwan, I. Iqra, S.S.A. Gillani, I. Zeba, M. Shakil, Z. Usman, PhSS 63 (2021) 134-140; https://doi.org/10.1134/S1063783421010182

[19] Y. Kanemitsu, T. Yamada, T. Handa, M. Nagai, Semicond. Sci. Technol. 35 (2020) 1-4; https://doi.org/10.1088/1361-6641/ab95b1

[20] H. Zhang, R. Li, Z. Cai, Z. Gu, A.A. Heidari, M. Wang, H. Chen, M. Chen, Expert Syst. Appl. 159 (2020) 1-7; https://doi.org/10.1016/j.eswa.2020.113617

[21] W. Kohn, Rev. Mod. Phys. 71 (1999) 1253-1266; https://doi.org/10.1103/RevModPhys.71.1253

[22] M. Riaz, B. Ali, S.M. Ali, M.I. Khan, M.S.U. Sahar, M. Shahid, M. Alam, J. Comput. Electron. 23 (2024) 483-497; https://doi.org/10.1007/s10825-024-02166-5

[23] S.S.A. Gillani, N. Fatima, I. Zeba, M. Shakil, R. Kiran, M.B. Tahir, M. Rizwan, R. Ahmad, A. Jawad, Mol. Simul. 47 (2021) 1549-1557; https://doi.org/10.1080/08927022.2021.1992406

[24] Y. Xu, S. Wu, L. Zhang, L. Wu, C. Ding, First-principles study of structural, electronic, elastic, and optical properties of cubic KNbO 3 and KTaO 3 crystals, 254 (2017) 1-10; https://doi.org/10.1002/pssb.201600620

[25] I.B. E, B.M. I, NIPES J. Sci. Technol. Res. 4 (2022) 324-333.

[26] Q. Mahmood, M. Hassan, S.H.A. Ahmad, A. Shahid, A. Laref, J. Phys. Chem. Solids 120 (2018) 87-95; https://doi.org/10.1016/j.jpcs.2018.04.024

[27] S. Bouhmaidi, A. Azouaoui, N. Benzakour, A. Hourmatallah, L. Setti, Comput. Condens. Matter 33 (2022) e00756; https://doi.org/10.1016/j.cocom.2022.e00756

[28] A.H. Reshak, M. Jamal, J. Alloys Compd. 543 (2012) 147-151; https://doi.org/10.1016/j.jallcom.2012.07.107

[29] M. Roknuzzaman, K. (Ken) Ostrikov, K. Chandula Wasalathilake, C. Yan, H. Wang, T. Tesfamichael, Org. Electron. 59 (2018) 99-106; https://doi.org/10.1016/j.orgel.2018.04.051

[30] V. Ashwin, M.S.S. M, M.B. Ahamed, S.B. Elavarasi, Appl. Phys. A Mater. Sci. Process. 126 (2020) 1-11; https://doi.org/10.1007/s00339-020-03977-6

[31] Y. Nassah, A. Benmakhlouf, L. Hadjeris, T. Helaimia, R. Khenata, A. Bouhemadou, S. Bin Omran, R. Sharma, S. Goumri Said, V. Srivastava, Bull. Mater. Sci. 46 (2023); https://doi.org/10.1007/s12034-023-02890-x

[32] E. Benrezgua, A. Zoukel, B. Deghfel, A. Boukhari, R. Amari, S. Kheawhom, A.A. Mohamad, A review on DFT + U scheme for structural, electronic, optical and magnetic properties of copper doped ZnO wurtzite structure, 2022; https://doi.org/10.1016/j.mtcomm.2022.103306

[33] M.H. Rahman, M. Jubair, M.Z. Rahaman, M.S. Ahasan, K. (Ken) Ostrikov, M. Roknuzzaman, RSC Adv. 12 (2022) 7497-7505; https://doi.org/10.1039/D2RA00414C

[34] A. Abdullah, S.M.J. Zaidi, M.I. Khan, M.S.U. Sahar, A.S. Saleemi, Comput. Condens. Matter 35 (2023) e00804; https://doi.org/10.1016/j.cocom.2023.e00804

[35] S. Gao, W. Li, J. Dai, Q. Wang, Z. Suo, Mater. Res. Express 8 (2021) 1-20; https://doi.org/10.1088/2053-1591/abde10

[36] A. Dey, R. Sharma, S.A. Dar, I.H. Wani, Comput. Condens. Matter 26 (2021) 2021-2023; https://doi.org/10.1016/j.cocom.2020.e00532

[37] M. Roknuzzaman, C. Zhang, K. (Ken) Ostrikov, A. Du, H. Wang, L. Wang, T. Tesfamichael, Sci. Rep. 9 (2019) 1-7; https://doi.org/10.1038/s41598-018-37132-2

[38] R. Brydson, B.G. Williams, W. Engel, H. Sauer, E. Zeitler, J.M. Thomas, Solid State Commun. 64 (1987) 609-612; https://doi.org/10.1016/0038-1098(87)90792-7

[39] F. Hofer, F.P. Schmidt, W. Grogger, G. Kothleitner, IOP Conf. Ser. Mater. Sci. Eng. 109 (2016) 8-11; https://doi.org/10.1088/1757-899X/109/1/012007

[40] M. Born, Math. Proc. Cambridge Philos. Soc. 36 (1940) 160-172; https://doi.org/10.1017/S0305004100017138

[41] Abdullah, U.A. Khan, I. Ullah, V. Tirth, A. Algahtani, Shazia, A. Zaman, Phys. Scr. 97 (2022); https://doi.org/10.1088/1402-4896/ac8292

[42] N.A. Noor, Q. Mahmood, M. Rashid, B. Ul Haq, A. Laref, Ceram. Int. 44 (2018) 13750-13756; https://doi.org/10.1016/j.ceramint.2018.04.217

[43] S. Al-Qaisi, M.A. Ali, T.A. Alrebdi, T. V. Vu, M. Morsi, B. Ul Haq, R. Ahmed, Q. Mahmood, S.A. Tahir, Mater. Chem. Phys. 275 (2022) 125237; https://doi.org/10.1016/j.matchemphys.2021.125237

[44] A. Bakar, A.O. Alrashdi, M.M. Fadhali, A. Afaq, H.A. Yakout, M. Asif, J. Mater. Res. Technol. 19 (2022) 4233-4241; https://doi.org/10.1016/j.jmrt.2022.06.126

[45] S. Tariq, A. Ahmed, S. Saad, S. Tariq, AIP Adv. 5 (2015) 1-20; https://doi.org/10.1063/1.4926437

[46] S. Ganeshan, S.L. Shang, H. Zhang, Y. Wang, M. Mantina, Z.K. Liu, Intermetallics 17 (2009) 313-318; https://doi.org/10.1016/j.intermet.2008.11.005

[47] M.I. Khan, S.M.J. Zaidi, M.S.U. Sahar, S.S.A. Gillani, M.A. Qaisrani, M.U. Farooq, J. Electron. Mater. 52 (2023) 5631-5641; https://doi.org/10.1007/s11664-023-10484-w

[48] W. Ren, J. Chen, G. Zhang, Appl. Phys. Lett. 121 (2022) 10-11; https://doi.org/10.1063/5.0106676

[49] D. Behera, S.K. Mukherjee, Chem. 4 (2022) 1044-1059; https://doi.org/10.3390/chemistry4030071

[50] M. Bilal, Saifullah, M. Shafiq, B. Khan, H.A. Rahnamaye Aliabad, S. Jalali Asadabadi, R. Ahmad, I. Ahmad, Phys. Lett. Sect. A Gen. At. Solid State Phys. 379 (2015) 206-210; https://doi.org/10.1016/j.physleta.2014.11.016

[51] A. Haoui, M. Elchikh, S. Hiadsi, Physica B : Condensed Matter 654 (2023) 4-8; https://doi.org/10.1016/j.physb.2023.414732

[52] D.S. Tsvetkov, M.O. Mazurin, V. V. Sereda, I.L. Ivanov, D.A. Malyshkin, A.Y. Zuev, J. Therm. Anal. Calorim. 147 (2022) 12661-12667; https://doi.org/10.1007/s10973-022-11480-8

[53] S. Saha, T.P. Sinha, A. Mookerjee, J. Phys. Condens. Matter 12 (2000) 3325-3336; https://doi.org/10.1088/0953-8984/12/14/309